Structural performance of bolted overlap connection in multi-span cold-formed steel Z-purlin

Ahmad Esam[1], Sherif Mourad[2], Maged Hanna[3], Amr Ibrahim[4]

[1]Teaching Assistant, Department of Civil Engineering, BUE, Egypt
E-mail: ahmad.esam@bue.edu.eg
[2]Professor, Structural Engineering Department, Cairo University, Egypt
E-mail: smourad@eng.cu.edu.eg.
[3]Professor, Structure and Metallic Construction Dept., HBRC, Egypt
E-mail: maged.tawfick@hbrc.edu.eg
[4]Lecturer, Department of Civil Engineering, BUE, Egypt
E-mail: Amr.ibrahim@bue.edu.eg

ABSTRACT

Recently, the use of Cold-Formed Steel (CFS) sections in construction has observed a significant surge. The connections of CFS buildings, in many instances, dictate their behaviour. This research aims to investigate the structural performance of overlap connections in multi-span CFS Z-purlin under monotonic loading. An overlap bolted connection is proposed for a multi-span continuous purlin system to achieve economic benefits while ensuring shear and moment transmission without pre-mature connection failure. The effects of overlap length and bolt arrangement were investigated in terms of flexural capacity and stiffness. Three specimens were experimentally tested, in which purlins made up of CFS Z-sections and high strength bolts *(HSB)* with a diameter of 12 mm and grade 8.8 were used. The test setup consisted of two-span back-to-back CFS Z-specimens connected using an overlap connection, with a point load applied at each span. The setup was designed with lateral supports to prevent lateral torsional buckling. The experimental results revealed that increasing the overlap length improved the flexural behaviour of the specimens. Moreover, the bolt arrangement was crucial to enhancing both the strength and stiffness of the lapped connections.

Keywords: Cold-formed sections, Overlap connections, Purlin Z-sections, Experimental testing, Semi-rigid connections.

INTRODUCTION:

Cold Formed Steel (CFS) sections have been established nowadays in the construction of steel buildings. They are made up of materials that have lightweight and high strength-to-weight ratios. Due to the flexibility in application, ease of fabrication and installation, they are most suitable for the construction of buildings. They could be implemented in buildings as secondary systems such as purlins, in which their main use is to transfer floor or roof loads to the main structural elements in low-to-medium-rise buildings. Furthermore, several types of CFS wall and roof systems have been involved in construction nowadays. However, the most popular system used is a multi-span Z-purlin section with overlapping connections. This system is popular due to its ease of installation as well as its high structural efficiency. Therefore, the recognition of the structural behavior of this overlapping connection system is required to achieve efficient modern system construction [1].

In the multi-span Z-purlin system, there is no engineering data that has been proposed to state the requirement of overlap connection to obtain moment capacity as connected section capacity in the CFS Z-purlin system. The connection is required to transmit shear and moment forces between multi-Z-purlins and their supports. The connection is typically semi-rigid and controls the section efficiency and the ability of Z-sections to reach their ultimate capacities. Furthermore, the semi-rigid connections will result in redistribution of moments, leading to reducing the bending moments at the hogging region, and consequently reducing the weight of the required sections. By implementing a continuous purlin system, it is possible to achieve significant savings on the cost of purlins in a steel building.

Previous studies on the flexural capacity of CFS and its influence on the behaviour of purlin overlapped connections have been conducted [2-4]. An advanced finite element analysis has been conducted on flexural capacity of Z-purlin system overlaps connection using ABAQUS. The results showed that all connections display semi-rigid behaviour. Further, increasing lap length has the greatest effect on the member's stiffness and resistance. In addition, designing the connection to avoid failure at the lap's edge increases stiffness and resistance significantly. Moreover, the moment capacity of the test specimen with an overlap length greater than 300 mm is higher than that of the control specimen. Finally, connecting the bottom flanges with screws has a significant effect only for short overlaps *Lp=100mm* in which the free flange deforms early.

Experimental investigations to study the behaviour of purlin connections in CFS Z-purlins have been conducted [5-7]. Tests were done on CFS Z-section with overlap and sleeve connections, with various overlap lengths, bolt configurations, web and flange stiffening, and epoxy resin to join the lapping. The results revealed overlapping connections are more efficient than sleeve connections. Furthermore, both types of connections failed due to distortional buckling. In addition, in the bolted overlap connection specimen, lower flange buckling, and web separation were detected.

Additionally, several researches investigated the behaviour of CFS sections used in portal and gable frames [8-11] and presented the performance of the corner or apex connection under static or dynamic loading. The results revealed that increasing the spacing between bolts has resulted in an increase in the moment capacity of the connection. Furthermore, the bolted connection has exhibited both the highest moment capacity and desirable ductile behavior when compared to screw connections. The findings also indicate that increasing the gusset plate thickness enhances the moment capacity of the connection and reduces displacement. Overall, the bolted specimens outperform the screw specimens.

This research focuses on the performance of bolted lap splice for CFS Z-shaped purlins and investigates the effect of the lap length and bolt arrangement on the connection moment capacity and failure modes.

EXPERIMENTAL SETUP

A total of three specimens were experimentally tested. As the Z-section is unsymmetrical, and in order to eliminate the torsion effect of asymmetric loading, a set of two Z-sections facing each other was tested. The two CFS Z-sections were connected with another two CFS Z-sections at overlap length (*Lp*) using *HSB* M12 of grade 8.8. The cross-section of the Z-Section was 200 mm high, having a top flange width of 60 mm, bottom flange width of 67 mm, lip depth of 20 mm and thickness of 3 mm (Figure 1). All three tests consisted of a two-span test setup with a span of 1500 mm, rested over 3 supports. Two-point loads were applied to the set-up with a distance of 600 mm from mid-support as shown in Figure 2. The first and second tested specimens, SP01 and SP02, had an overlap length (*Lp*) of 300 and 600 mm, respectively, with HS bolts M12 (8.8) used in the web as shown in Figures 3(a) and 3(b). The third and last tested specimen (SP03) had an overlap length (*Lp*) of 600 mm, with HS bolts M12 (8.8) connecting both web and flange as shown in Figure 3c.

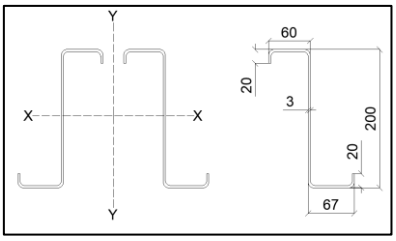

Figure 1: Tested CFS Z-section dimensions (in mm).

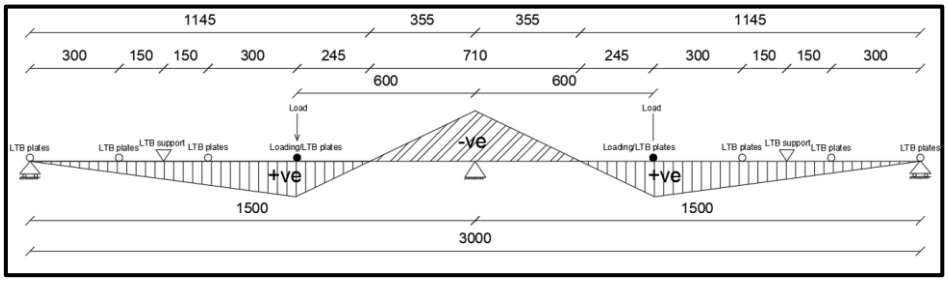

Figure 2: Schematic drawing for expected bending moment for continuous two-spans, location of load application & LTB support location assuming fully-rigid lap splice.

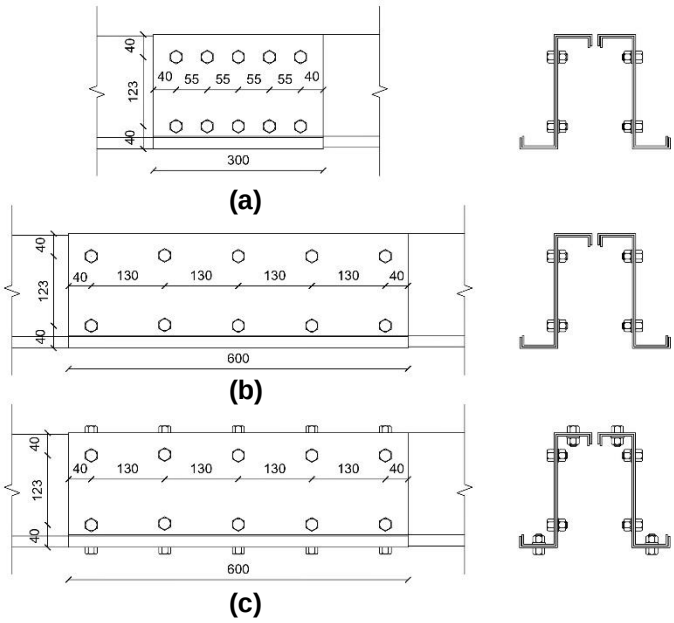

Figure 3: Specimens overlap connection dimension (a) SP01 connection, (b) SP02 connection, & (c) SP03 connection (all dimensions in mm's).

MATERIAL PROPERTIES:

Steel S355 was specified for the purlin material. However, in order to determine the exact mechanical properties, a total of 3 coupon tests were performed. Dimensions of the coupons and the test procedure were according to the ASTM-A370 specifications [12]. Two coupon tests were extracted from the web of the CFS Z-section (CT01 & CT02), and one coupon test was extracted from the flange of the CFS Z-section (CT03). The three samples were tested using a universal machine as shown in Figure 4. The failure of the coupon test is shown in Figure 5. The stress-strain curve for the 3-coupon tensile test is shown below in Figure 6. The coupon test results are shown in Table 1.

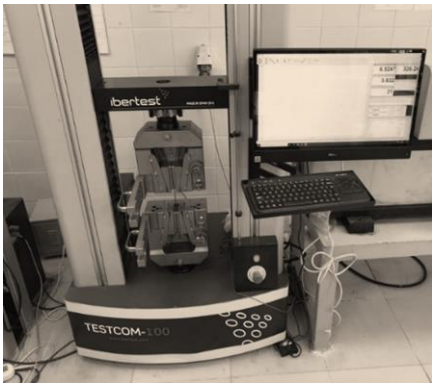

Figure 4: Coupon tension test using the universal machine.

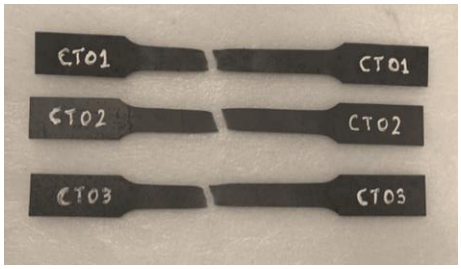

Figure 5: Failure of coupon test (Cup and cone failure).

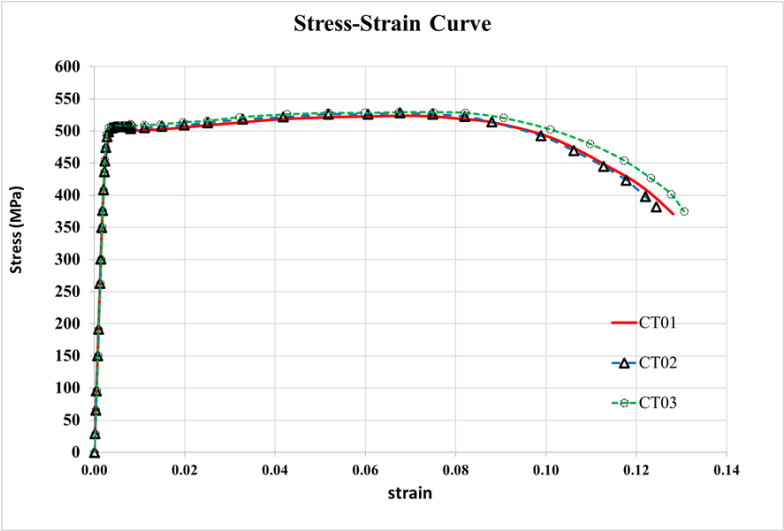

Figure 6: Stress-strain curve for coupon tests.

Table 1: Steel properties for tested coupon test.

Specimen ID	Yield strength (MPa)	Yield strain (ε_y) %	Ultimate strength (MPa)	ultimate strain (ε_u) %	Fracture strain (ε_f) %	Modulus of elasticity *(E)* GPa
CT01	348.4	0.169	524.0	6.88	12.82	205.9
CT02	350.1	0.167	528.5	6.76	11.28	209.9
CT03	350.7	0.168	529.6	6.74	13.05	208.4

In addition, for bolt connection properties, a lap joint shear test has been performed to determine the failure type of connection, whether it is the bearing of plates or the shear failure of bolts. The dimensions of the lap joint shear test and the testing of specimens are shown in Figure 7 & Figure 8, respectively. A high strength bolts of grade 8.8 with a diameter of 12 mm have been used. A total of three lap joint shear test has been established and failure was always due to bearing failure in plates as shown in Fig. 9. The results of the lap joint test are shown in Table 2.

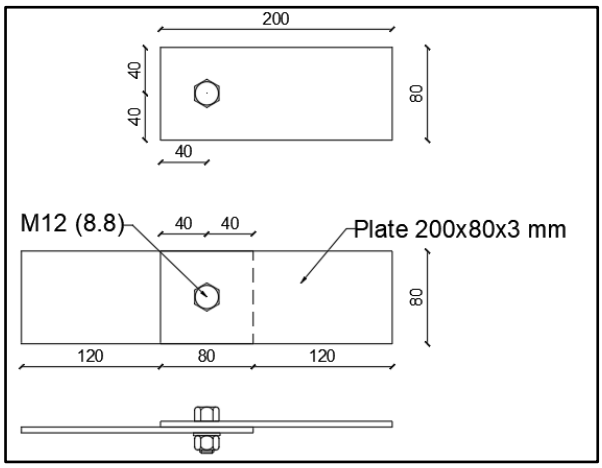

Figure 7: Dimensions of Lap joint shear test.

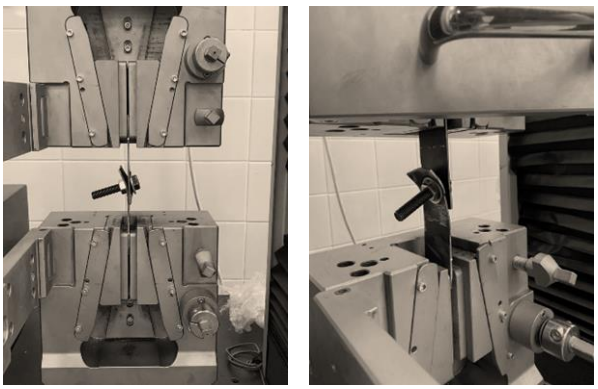

Figure 8: Lap joint shear test.

Figure 9: Failure mode of lap joint shear specimens.

Table 2: Lap joint shear test results.

Specimen ID	Yield strength (MPa)	Ultimate strength (MPa)	elongation %
ST01	179.31	190.79	11.41
ST02	187.43	187.43	16.23
ST03	187.81	188.39	14.81

TEST SETUP AND PROCEDURE.

The test setup of all three specimens consisted of two continuous spans Z-section with an overlap length resting over an I-shaped rigid beam (HEB with circular solid welded to top flange acting as a roller) as shown in Figure 10-11. The loading jack was employed to apply load on the beam which distributes the load on each span at a distance of 600mm from the middle support as shown in Figure 10-11. The boundary conditions used at the two ends and middle are roller supports.

Further, linear variable differential transformers (LVDTs) were used to measure displacement. For all three specimens, (LVDTs) were used under the loading points. Further, in the SP02 test setup, LVDTs were used near end support to measure the angle of rotation (deflection slope) at end support. On the other hand, in SP01 & SP03 test setups, LVDTs were used before and after overlapping connection to measure the angle of rotation (deflection slope) due to a hogging moment at mid-support.

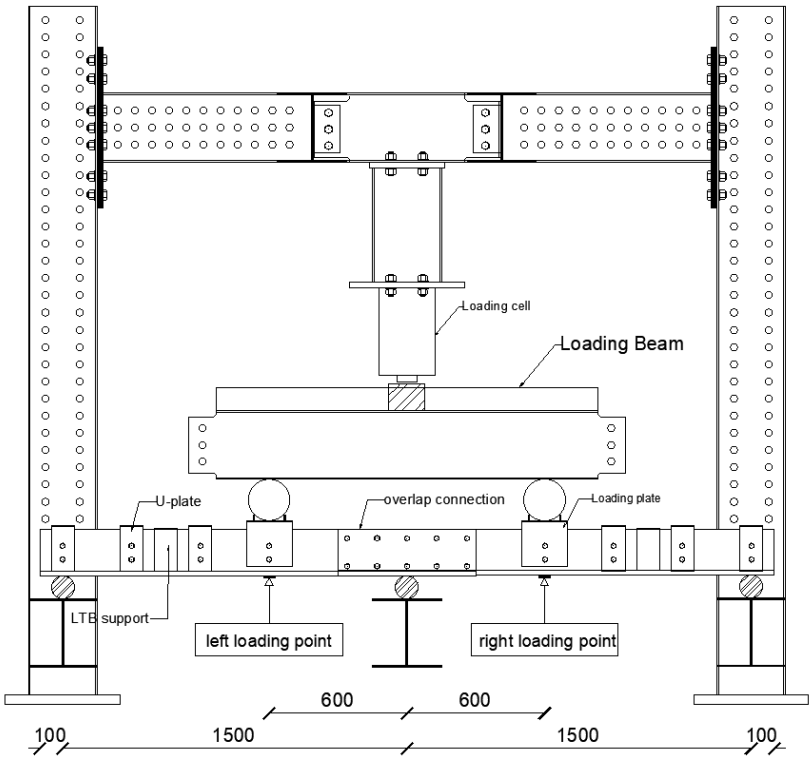

Figure 10: A schematic of the test setup (all dimensions in mm's).

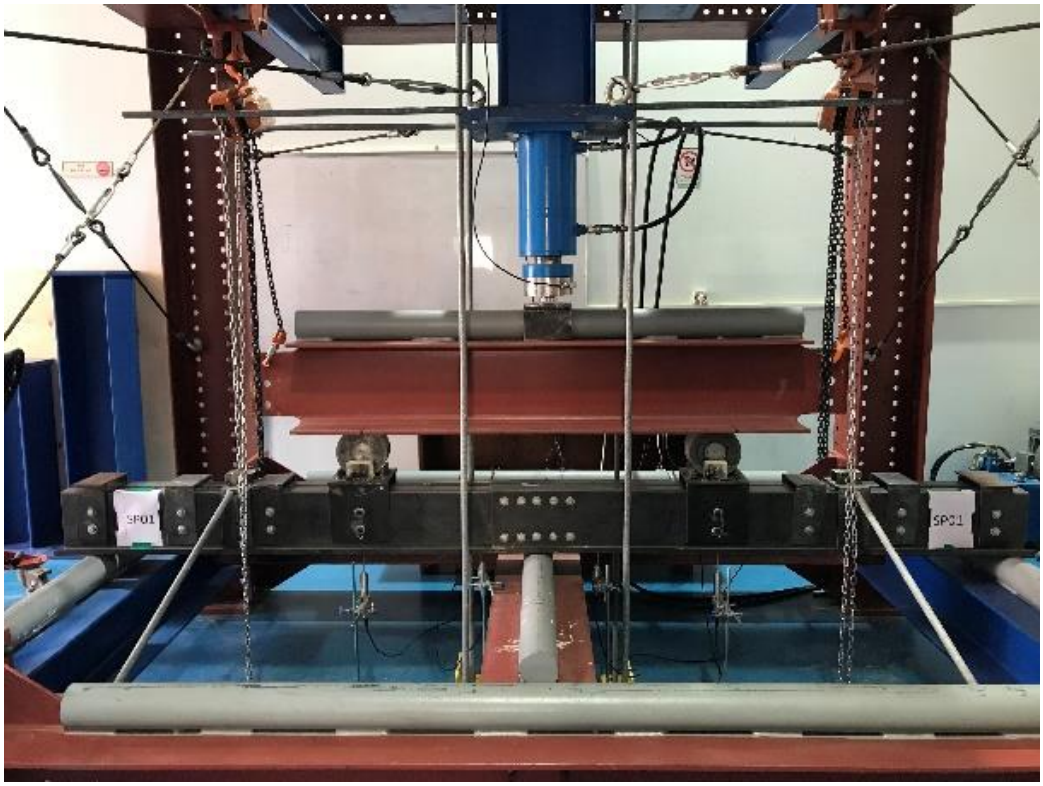

Figure 11: Actual configuration of experimental test setup.

RESULTS AND DISCUSSION:

The results of the three experimental specimen tests are illustrated and explained in detail. The outcome of the experiment is expressed for each of the two-loading point, as illustrated in Figure 10. Two load-displacement curves are plotted for each experiment test, one for the left loading point and the other for the right loading point. Further, using the maximum jack load for each experimental test result, a moment capacity for connection is determined based on the relation between the load applied and the moment. By analyzing the portal frame using SAP2000 V20 software, a correlation is established between the Jack load values acquired through experimental and numerical analysis and the moment achieved at the single purlin overlap connection. This is achieved by applying a two-point load at each span with a magnitude of 1 kN at a distance of 600 mm from middle support as shown in Figure 12. The value for the moment at mid-support corresponding to the load applied is shown as well (0.26 kN.m).

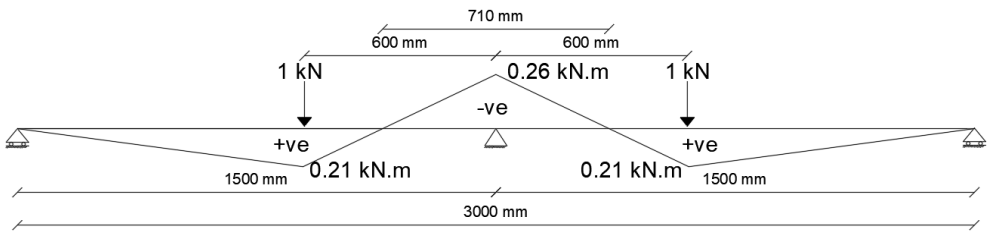

Figure 12: Relation between the loading cell values and connection moment capacity of purlin overlap connection.

- The bending moment at overlap connection = 0.258 x point load applied
- Where point load = Jack load /4
- Therefore, the Bending moment at single overlap connection =0.0645 x jack load

Finally, the rotation of the overlap connection from each side (left and right) is determined based on the assumed linear relation between displacement and rotation. It is assumed that there is a linear relationship between the rotation of the overlap connection and the vertical displacement at the location of loading on the purlin. which corresponds to each load identified through either numerical or experimental testing. The calculation of the overlap connection's rotation is demonstrated in Figure 13.

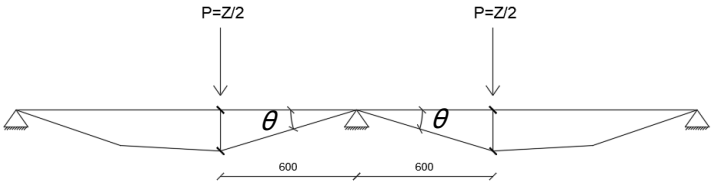

$$The\ rotation\ angle\ at\ overlap\ connection\ (\theta) = (\Delta\ (in\ mm))/600$$

Figure 13: Relation between the displacement values and rotation of overlap connection

SP01 experimental results.

Specimen SP01 connected the CFS Z-section with an overlap length of 300 mm using HSB M12 (8.8) in the web only. The deformation of SP01 is shown in Figure 14, with buckling observed in the top & bottom flange at the end of the overlap connection. Further, the failure mode of the specimen is illustrated in Figure 15. It can be observed that there is a separation between the top flanges at the overlap connection. Regarding the connection, no bearing damage occurred, and the bolts remained intact. It is noticed that the specimen failed due to distortional buckling at the overlap connection. Additionally, the failure of the specimen occurred at maximum flexural capacity of 11.88 kN.m, with corresponding rotation at the left and right spans of 0.0100 and 0.0121 radian angle, respectively.

Figure 14: Deformation of SP01 specimen.

Figure 15: SP01 failure mode.

SP02 experimental results.

Specimen SP02 connected the CFS Z-section with an overlap length of 600 mm using HS bolts M12 (8.8) in the web only. The deformation of SP02 is shown in Figure 16. It can be observed

that there is a buckling in the top & bottom flange at the end of the overlap connection. Moreover, the failure mode of SP02 is depicted in Figure 17, indicating that there is a separation between the top flanges at the overlap connection. As noticed, failure was initiated as local buckling of the bottom flange of overlap connection followed by local buckling of the cross section under the loading point. Additionally, the failure of the specimen occurred at maximum flexural capacity of 12.47 kN.m, with corresponding rotation at the left and right spans of 0.0110 and 0.0122 radian angle, respectively.

Figure 16: Deformation of SP02 specimen.

Figure 17: SP02 failure mode.

SP03 experimental results.

Specimen SP03 had the CFS Z-sections connected with an overlap length of 600 mm using HS bolts M12 (8.8) in both web and flange. Figure 18, illustrates the deformation of the SP03 specimen. It can be observed that there is a buckling in the top & bottom flange left and right of the overlap connection. Further, it has been observed that there is no separation between the flanges at the overlap connection. In addition, the failure mode of the specimen is shown in Figure 19, indicating that failure occurred due to local buckling of the cross section under the loading point and the connection almost buckled. Moreover, the specimen reached maximum flexural capacity of 13.18 kN.m, with corresponding rotation at the left and right spans of 0.0107 and 0.0121 radian angle, respectively.

Figure 18: Deformation of SP03 specimen.

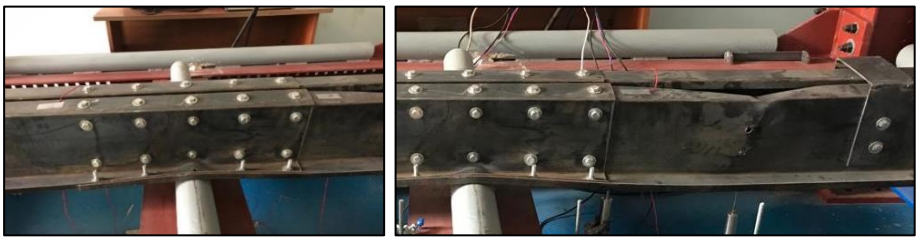

Figure 19: SP03 failure mode.

Comparison between tested specimens.

The ratio of connection to section moment capacity (Ms/Mc) versus rotation of specimen are plotted against each other for left point and right points as shown in Figs. 20 and 21,

respectively. The finite element modeling software Abaqus [13] has been utilized to ascertain the moment capacity of the Z section with double thickness at the position of the proposed overlap connection. The experimental results of all specimens showing the maximum load capacity and corresponding displacements at left & right loading points are shown in Table 3. Additionally, the connection and section moment capacities, as well as the ratios between them, in addition to the rotations in connections, are shown in Table 4.

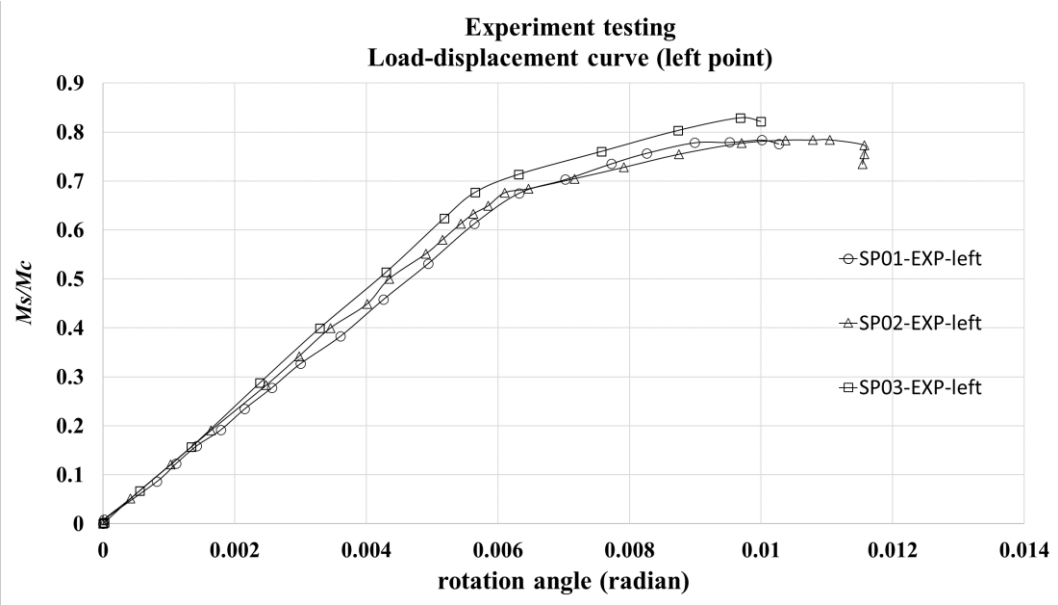

Figure 20: Ratio of connection to section moment capacity versus rotation of specimen (left point).

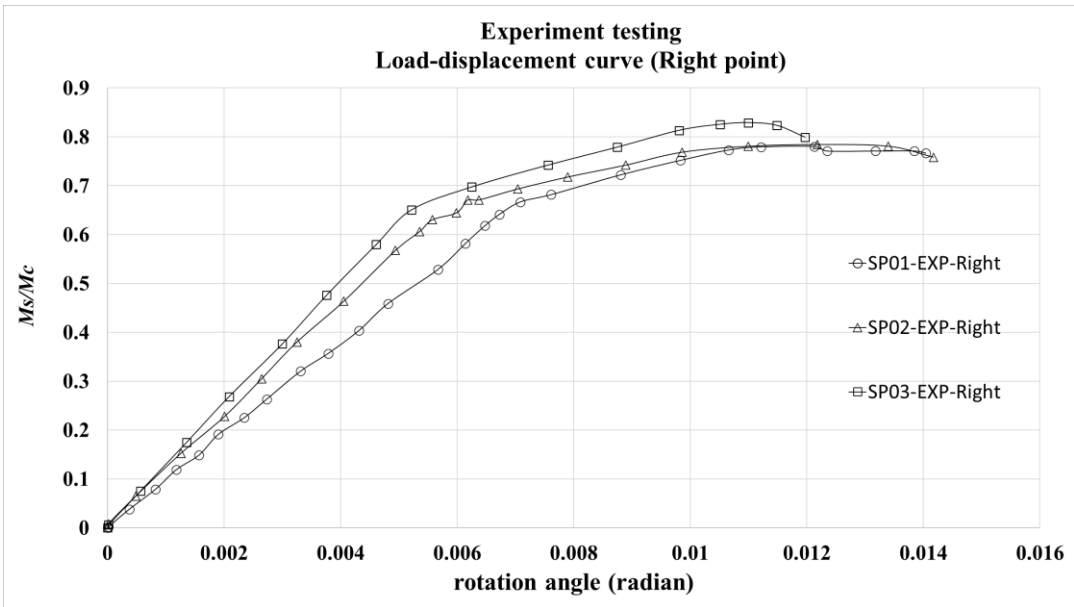

Figure 21: Ratio of connection to section moment capacity versus rotation of specimen (right point).

Table 3: Experimental results for all specimens.

model	Jack Load (kN)	Left displacement (mm)	Right displacement (mm)
SP01	184.13	6.01	7.28
SP02	193.33	6.63	7.31
SP03	204.38	5.81	6.60

Table 4: The connection capacity, section moment capacity, and the rotations in connections.

model	Connection Capacity *(Ms)* KN.m	Section Capacity *(Mc)* KN.m	*Ms/Mc*	Left span rotation *(θ_L)*	Right span rotation *(θ_R)*
SP01	11.88	15.90	0.747	0.0100	0.0121
SP02	12.47	16.75	0.744	0.0110	0.0122
SP03	13.18	16.75	0.787	0.0107	0.0121

CONCLUSIONS:

1. In the specimen with overlap length/section depth (*Lp/d)* of 1.5 and a web-bolted connection, the dominant failure mode was local buckling of the overlap connection. This means that the failure occurred in the connection rather than the cross section indicating that the connection was not able to fully transmit the moment.
2. In the specimen with a (*Lp/d)* of 3 and a web-bolted connection, the failure was initiated by local buckling of the flanges at the overlap connection, followed by buckling of the cross-section under the loading point, although the connection was capable of transmitting the moment.
3. Specimen with (*Lp/d)* of 3 and overlap connection bolted in both the flanges and webs, failure mode was governed by the failure of the cross-section under the loading point, indicating the connection was capable of transmitting moment between cross-sections.
4. Increasing the ratio of overlap length to section depth (*Lp/d)* from 1.5 to 3, has caused an increase in connection moment capacity by 4.88%. On the other hand, deflection has increased by an average value of 5.11%.
5. Using bolts to connect both the flanges and webs at the overlap connection enhanced the connection moment capacity by 5.55% and increased deflection by an average value of 2.15 %, relative to overlap connection with webs bolted only.
6. The highest ratio of the connection to the section moment capacity was 0.787, and it was achieved by an overlap connection bolted at both flanges and web, and with an Lp/d value of 3.

ACKNOWLEDGEMENT :

The experimental testing took place at Civil Structural Laboratory at the British University in Egypt (BUE). The permission to use the facilities and the help received from the lab staff is gratefully acknowledged.

REFERENCES

1. Yu, W. W., Laboube, R. A., & Chen, H. (2020). Cold-Formed Steel Design. In Wiley. https://doi.org/10.1007/978-1-4757-0411-2_9
2. Gîrbacea, I. A., & Ungureanu, V. (2021). Finite Element Analysis of Overlapped Z-Purlins Restrained by Sheeting. IOP Conference Series: Materials Science and Engineering, 1203(3), 032077. https://doi.org/10.1088/1757-899x/1203/3/032077
3. Gutiérrez, R. M., Loureiro, A., Reinosa, J. M., & Lopez, M. (2019). Numerical study of semi-rigid behaviour joints for slender purlins. Nordic Steel Construction Conference, 3(3–4), 225–230. https://doi.org/10.1002/cepa.1049.
4. Ho, H. C., & Chung, K. F. (2017). Advanced numerical investigation into structural behaviour of high-strength cold-formed steel lapped Z-sections with different overlapping lengths. Advances in Structural Engineering, 20(7), 1074–1097. https://doi.org/10.1177/1369433216670664
5. Young, B., & Ellobody, E. (2023). Experimental investigation on cold-formed steel Z-sections having different stiffened flanges undergoing web crippling. Engineering Structures, 286(June 2022), 116144. https://doi.org/10.1016/j.engstruct.2023.116144
6. Kavya, E., & Swedha, T. (2017). A Comparative Study on Experimental Behaviour Of Cold Formed Sigma and Z Section Purlin Connections. International Journal of Scientific & Engineering Research, 8(6), 1–7.
7. El-sayed, K., Khalil, N., & Zaky, A. (2015). Flexural Behavior of Lapped Connections in Multi-span Cold-formed Z-purlins. Advances in Research, 5(4), 1–16. https://doi.org/10.9734/air/2015/18797
8. Sherif A. Mourad, Maged T.Hanna, Hazem H. Elanwar, Ahmed M. Massoud, “Structural Performance of Cold Formed Sections Portal Frames Eave Connections with Different Fasteners (Screws / Bolts),” Proceedings of the Cold-Formed Steel Research Consortium Colloquium (cfsrc.org), 17-19 October 2022.
9. Sherif A. Mourad, Arwa M. Naguib, and Hazem H. Alanwar, “Numerical modelling of apex connections in cold-formed steel gable frames,” 14th International Conference on Civil and Architecture Engineering (ICCAE), March 2022.
10. Yasser N. Saleh, Hazem H. Elanwar, Maged T. Hanna, and Sherif A. Mourad, “Assessment of frame corner connections subjected to cyclic loading in cold formed steel sections,” Journal of Constructional Steel Research, 199 (2022) Article 107601, https://doi.org/10.1016/j.jcsr.2022.107601
11. Abdel-Rahman, M.H.Z., (2022). Laboratory testing and numerical modelling of frame apex connections fabricated from steel cold-formed sections, M.Sc., Faculty of Engineering, Cairo University.
12. ASTM A370, Standard Test Methods and Definitions for Mechanical Testing of Steel Products, 2019.
13. ABAQUS, Version 2020. Pawtucket, USA: Hibbitt, Karlsson & Sorensen, Inc., 2020.